



Contents lists available at ScienceDirect

# Journal of Quantitative Spectroscopy & Radiative Transfer

journal homepage: [www.elsevier.com/locate/jqsrt](http://www.elsevier.com/locate/jqsrt)

## Self- and air-broadened cross sections of ethane (C<sub>2</sub>H<sub>6</sub>) determined by frequency-stabilized cavity ring-down spectroscopy near 1.68 μm

Zachary D. Reed\*, Joseph T. Hodges

Material Measurement Laboratory, National Institute of Standards and Technology, 100 Bureau Drive, Gaithersburg, MD 20899, USA



### ARTICLE INFO

#### Article history:

Received 29 October 2014

Received in revised form

21 January 2015

Accepted 9 March 2015

Available online 17 March 2015

#### Keywords:

Ethane

C<sub>2</sub>H<sub>6</sub>

Cavity ring-down spectroscopy

CRDS

Cavity enhanced spectroscopy

Methane monitoring

### ABSTRACT

The absorption spectrum of ethane was measured by frequency-stabilized cavity ring-down spectroscopy over the wave number range 5950–5967 cm<sup>-1</sup>. Spectra are reported for both pure ethane acquired at pressures near 3 Pa and mixtures of ethane in air at pressures ranging from 666 Pa to 101.3 kPa. Absorption cross sections are reported with a spectrum sampling period of 109 MHz and frequency resolution of 200 kHz. Atmospheric pressure cross sections agree fairly well with existing cross sections determined by FTS in nitrogen, but there are significant variations in cross sections at lower pressures. Source identification of fugitive methane emissions using spectroscopic measurements of the atmospheric ethane-to-methane ratio is also discussed.

Published by Elsevier Ltd.

### 1. Introduction

The gaseous hydrocarbon ethane (C<sub>2</sub>H<sub>6</sub>) is a contributor to photochemical pollution and ozone production. It is the second-most abundant hydrocarbon in the atmosphere behind methane (CH<sub>4</sub>). The atmospheric concentration of ethane varies widely, with a large disparity between the Northern and Southern hemispheres. The average molar fraction in the Northern hemisphere is near 1 nmol/mol, while in the Southern hemisphere it averages about 0.3 nmol/mol [1]. This compares to tropospheric methane (CH<sub>4</sub>) concentrations of around 1800 nmol/mol, which is well mixed in the atmosphere [2].

Although ethane has a minor direct radiative forcing effect, it has a significant impact on air quality. The atmospheric lifetime of ethane is two months [1], which prevents complete mixing in the atmosphere and leads

to higher concentrations in the lower troposphere. Atmospheric oxidation of ethane leads to the formation of byproducts including formaldehyde [3], carbon monoxide [3], and peroxyacetyl nitrate, which is a reservoir for NO<sub>x</sub> [4]. Tropospheric ozone is also produced by the oxidation of hydrocarbons, including ethane [5].

There is considerable uncertainty in the emission budget and sources of ethane [6]. Three-dimensional chemical transport models give estimates of the global inventory from 12 to 13.5 Tg yr<sup>-1</sup> [7–9], and a recent study indicates that the concentration has been decreasing since 1984 [1]. Emission sources, which include the oceans, and various biogenic and anthropogenic sources, have been estimated, but the uncertainties are large [10,11]. Sources can be distinguished by the ratio of ethane to methane as well as by the ratio of ethane to larger hydrocarbons such as propane (C<sub>3</sub>H<sub>8</sub>) [12]. Fugitive emissions from pipelines and drilling sites are one of the largest anthropogenic sources of ethane and are a particular concern [1,13]. Indeed, methane source apportionment is a significant motivation for ethane sensor development.

\* Corresponding author. Tel.: +1 301 975 2422; fax: +1 301 975 3670.  
E-mail address: [zachary.reed@nist.gov](mailto:zachary.reed@nist.gov) (Z.D. Reed).

Ethane is also a species of astrophysical interest and has been detected in the atmospheres of the gas giant planets [14,15], the largest moon of Saturn (i.e., Titan) [16–18], and several comets [19]. The Cassini [15] probe obtained spectroscopic measurements of ethane at several wavelengths, including 1.64  $\mu\text{m}$ . However, it suffered a malfunction and data from the 1.64  $\mu\text{m}$  band was corrupted. This band would have provided additional information about the optical depth of the ethane clouds on Titan.

Spectroscopic measurement techniques are frequently used for concentration determination of methane and ethane. Fourier transform spectroscopy (FTS) has been widely used to determine spectroscopic parameters of ethane [20] and has been used for field-concentration determination of methane [12]. Spectroscopic studies have focused on the mid-infrared region of the spectrum, with relatively few investigations on the overtone range above 3000  $\text{cm}^{-1}$ . A medium-resolution survey of the spectrum up to 6000  $\text{cm}^{-1}$  was obtained in 1949 by Smith [21] at room temperature and relatively high pressure. More recently, a survey spectrum of ethane in nitrogen was obtained from 600 to 6600  $\text{cm}^{-1}$  at atmospheric pressure by FTS [22] and absorption cross sections were reported. Overtone spectra of jet-cooled ethane in the region 4000–6500  $\text{cm}^{-1}$  have been studied by FTS at fairly high resolution [23,24]. The spectrum has a high density of vibrational levels, with numerous perturbations, making line-by-line assignment difficult. Nevertheless, jet-cooling of ethane samples has allowed for detailed assignments to be made from 4000 to 4500  $\text{cm}^{-1}$  [24].

The existing spectroscopic measurements suffer from some significant limitations. The PNNL database measurements were made of nitrogen-broadened ethane at atmospheric pressure. Additionally, the spectra feature negative cross sections in the region around 1.6  $\mu\text{m}$ , indicating some error in the determination of the instrument baseline. To our knowledge, no FTS determinations of cross sections utilizing high resolution FT instrumentation and at various sample pressures have been published in this wavelength region. Previous field measurement campaigns have employed flask sampling and GC–MS analysis for determination of atmospheric ethane concentrations [1,12]. The uncertainties are large and cannot be performed in the field. Laser spectroscopic techniques offer an alternative for field measurements. Studies have been performed using tunable diode laser spectroscopy [25], multi-pass laser techniques [26], and with resonant optical techniques like cavity ring-down spectroscopy [27–30]. Most of these techniques rely on mid-infrared lasers to achieve adequate sensitivity, although these light sources are expensive and may be complicated to use.

Commercially available continuous-wave, near-infrared lasers offer a robust, relatively inexpensive and attractive alternative. In the remainder of this article, we present a high-resolution study of the ethane spectrum near 5950  $\text{cm}^{-1}$  using frequency-stabilized cavity ring-down spectroscopy (FS-CRDS), and we discuss atmospheric sensing applications. A complete list of all the measured absorption cross sections, which are presented below, for both pure ethane and ethane in air, can be found in the [Supplementary information](#).

## 2. Experimental apparatus

All measurements were performed using a FS-CRDS system at the National Institute of Standards and Technology (NIST) in Gaithersburg, MD. Because the FS-CRDS technique has been described in detail in previous work [31–33], we provide only a brief summary.

The probe laser is a single-mode, continuous-wave external cavity diode laser (ECDL) with a linewidth of 1 MHz and wavelength of 1.68  $\mu\text{m}$ . The ECDL output is amplified to 30 mW with a booster optical amplifier (BOA). The ring-down spectrometer comprises two highly reflective mirrors ( $R=0.999\,960$  at the probe wavelength, cavity finesse of 78,000) to create a high finesse optical cavity. The ring-down cavity mirrors are also partially reflective at a wavelength of 0.633  $\mu\text{m}$  to enable active locking of the cavity length (139 cm) to an iodine-stabilized HeNe laser having a long term frequency stability of 10 kHz. The cavity length stabilization creates a comb of resonant cavity modes separated by the free spectral range (FSR=108.750(2) MHz at vacuum) of the cavity. At each spectrum point, the probe laser frequency is actively locked to a mode of the ring-down cavity with a proportional-integral scheme. The BOA is also used as an optical switch in order to initiate the decay events and typically decay signals are acquired at a rate of 200 Hz for each frequency step. The probe laser servo has a bandwidth of approximately 50 Hz and is realized using a high-precision (10 MHz resolution) and high-speed (400 MHz update rate) wavelength meter to measure frequency detuning about the target mode. Dithering the laser frequency and measuring the cavity transmission yields an analog error signal, which is fed back to the pzt-actuated fine frequency control of the ECDL. Although this servo is not rapid enough to narrow the laser linewidth, it eliminates drift of the laser frequency by maximizing the average transmission through the cavity. Successive spectrum points are acquired by breaking the ECDL lock, tuning to the next cavity mode and relocking. This mode-by-mode, step-scanning approach leads to a linear and precise frequency detuning axis, which we calibrate against an absolute reference as described below. Under continuously locked conditions, the resolution of the frequency axis is approximately 200 kHz and is limited by the precision of the probe laser locking servo. For a nominally mode-matched configuration, the FS-CRDS approach guarantees that only one cavity transverse mode can be excited at a given time because the mode spacing is much greater than the line width of the probe laser. Single-mode cavity excitation also results in exponential decay signals, which are characterized by a time constant that can be determined with relative uncertainties at the 0.05% level. For the present system, the minimum detectable absorption coefficient,  $\alpha_{\text{min}}$ , is  $10^{-11} \text{ cm}^{-1}$  based on 1 s averaging time (200 decay signals). Combined with the frequency axis precision, this allows for highly accurate measurements of absolute absorption quantities and line positions.

We model the time-dependent FS-CRDS decay signal  $s(t)$  as

$$s(t) = s_0 \exp(-t/\tau(\nu_j)) + s_b, \quad (1)$$

where  $\tau$  is the intensity decay time (determined by least-squares fits of the individual decay events) at the  $j$ th cavity mode frequency  $\nu_j$ , and  $s_b$  is a constant baseline. The absorption loss is modeled as

$$\frac{1}{c\tau(\nu_j)} = \alpha(\nu_j) + \frac{L_0(\nu_j) + \Delta L_e(\nu_j)}{l} \quad (2)$$

where  $c$  is the speed of light,  $l$  is the mirror-to-mirror distance,  $L_0 = 1 - \sqrt{R_1 R_2}$  is the mean cavity mirror loss,  $\Delta L_e$  is the contribution of etalons, which are manifest as sinusoidal variations in the base losses, and  $\alpha$  is the absorption coefficient of the sample. The mirror loss and etalon terms constitute the spectrum baseline. These quantities are measured in the empty cavity and subtracted to yield the corrected loss spectrum.

The absorption cross section is given by  $\sigma(\nu_j) = \alpha(\nu_j) k_B T / p x$ , where  $x$  is the molar fraction of the absorbing species,  $k_B$  is the Boltzmann constant,  $T$  and  $p$  are the sample temperature and pressure, respectively.

The absolute frequency axis is determined by measuring the heterodyne beat frequency of the probe laser against a Cs-clock-referenced optical frequency comb (OFC). This measurement is realized on the first spectrum point of each scan and yields an absolute uncertainty of approximately 200 kHz. The detuning relative to the first point of the scan is then determined from integer multiples of the known FSR, which introduces negligible uncertainty to the absolute frequency measurement. However, due to the length of some scans it was not possible to make the measurement while maintaining a cavity lock. In these cases we used the aforementioned wavelength meter for absolute frequency determination over portions of the spectra. This wavelength meter was calibrated against the heterodyne beat frequency between the locked probe laser and an optical frequency comb, yielding an uncertainty in the absolute frequency of nominally 5 MHz.

We measured the sample gas pressure with a capacitance diaphragm gauge having a relative standard uncertainty of 0.0015% at a full scale reading of 133 kPa. This gauge was calibrated against a NIST transfer standard apparatus. The transfer standard was employed directly for low pressure measurements to give a relative standard uncertainty of 0.15% at 3 Pa. The cell temperature was measured using a NIST-calibrated thermistor with a standard uncertainty of 0.02 K.

### 3. Spectroscopy

The infrared spectrum of ethane is dense and relatively complicated. There are 12 fundamental vibrations, which have been studied extensively [20,34–36]. The near-infrared vibrational overtones have received limited attention, largely due to the difficulty in making assignments. Smith [21] identified an overtone band centered at  $5948 \text{ cm}^{-1}$  and assigned it to the  $\nu_7 + \nu_{10}$  combination band. Cross sections for this wavelength region were obtained by FTS at Pacific Northwest Laboratory [22], but only for ethane in nitrogen at 101.3 kPa. This band was investigated further by Hepp [23] and six Q branches were assigned. These bands are promising for sensing applications because there is minimal

spectral interference with other atmospheric species, including most other hydrocarbons.

Here, we measured the progression of  ${}^r\text{Q}_n$  branches ( $n=0-2$ ) of the  $\nu_7 + \nu_{10}$  band. The measured spectra of pure ethane can be found in Fig. 1a, along with a comparison to the measured spectra of ethane in air ( $13.93 \pm 0.05 \mu\text{mol/mol}$   $\text{C}_2\text{H}_6$ , prepared at NIST) at 670 Pa. The pure ethane spectrum was measured at 2.86 Pa and 296.1 K, while the ethane-in-air spectrum was measured at 666 Pa and 296.0 K. The sampling period for both was 109 MHz, equivalent to the FSR of the ring-down cavity. The SNR, defined as the peak signal over the standard deviation of the empty-cavity spectrum baseline, exceeds 100,000 for the pure ethane spectrum and is  $\sim 550$  for the ethane in air spectrum. The relatively low ethane concentration and alignment-dependent variations in etalon amplitudes result in the lower SNR of the ethane-in-air spectrum. Nevertheless, many weak features are reproduced extremely well, giving additional confirmation that these correspond to real spectroscopic structures. The measured absorption cross sections and combined uncertainties of some noteworthy features can be found in Table 1.

As evident in Fig. 1, the Q-branches are sharp and well-resolved in these Doppler-limited spectra. The dense structure within the apparent baseline of the FS-CRDS spectrum is highly reproducible. Averaging over multiple spectra yields an intensity standard deviation of less than 0.1%, demonstrating that this structure corresponds to ethane absorption features and not noise in the spectrum. We note that we were unable to replicate the results of Oh et al. [28] in this spectral region. Due to the low uncertainty in our frequency axis, along with the close agreement of this work to available PNNL results (discussed later in this work), we believe that there was a substantial error in the frequency axis of Oh et al.

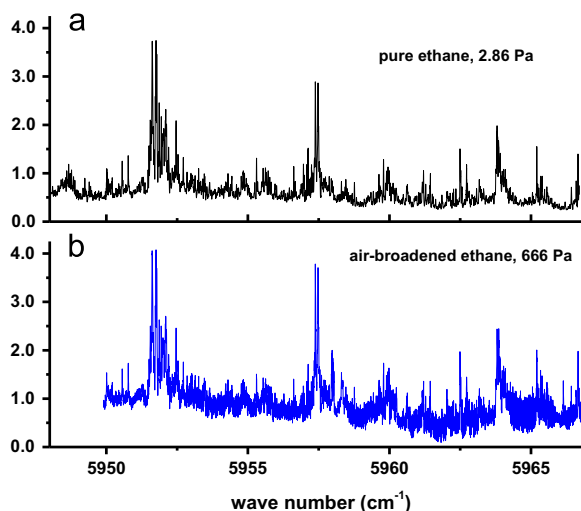


Fig. 1. Ethane spectra for self- and air-broadened cases. (a) Pure ethane measured by FS-CRDS at 2.86 Pa, (b) ethane in air ( $13.93 \pm 0.05 \mu\text{mol/mol}$ ) measured by FS-CRDS at 666 Pa. For these FS-CRDS spectra, the cavity lock was not continuously maintained, and consequently the accuracy of the frequency axis over the range covered was limited by the uncertainty of wavelength meter ( $\sim 5$  MHz).

**Table 1**Measured absorption cross sections in units of  $10^{-21} \text{ cm}^2 \text{ molecule}^{-1}$  for ethane at selected wave numbers.

Wavenumber ( $\text{cm}^{-1}$ )	Pure ethane	Ethane in air				
	2.86 (Pa)	666 (Pa)	1.333 (kPa)	6.666 (kPa)	39.996 (kPa)	101.325 (kPa)
5950.771	1.36	1.75	1.29	1.11		0.76
5951.755	3.74	4.11	3.45	3.14	2.22	1.81
5957.380	2.89	3.81				
5963.800	1.98	2.46				

The measured absorption cross section in the FS-CRDS spectrum of Fig. 1a and b has a significant pedestal and does not reach near zero absorption at any point in this wavelength region, even at very low pressures. This offset is present in pure ethane and ethane-in-air. This property significantly limits the dynamic range of the spectrometer in pure ethane measurements. The absorption intensity of the pedestal decreases to the red side of the band head located at  $5948 \text{ cm}^{-1}$ . For both pure ethane (0.13–40 Pa) and ethane-in-air mixtures (666 Pa–101.3 kPa), the absorption coefficient of the nominal baseline (at a given wavelength) is proportional to the ethane number density and corresponds to an effective baseline absorption cross section of  $\sim 5.4 \times 10^{-22} \text{ cm}^2 \text{ molecule}^{-1}$ . The pedestal alone was sufficient to exceed the dynamic range of the spectrometer at pure ethane pressures of higher than 40 Pa. Note that this pedestal is included in all reported cross sections.

Ethane-in-air spectra at pressures ranging from 0.666 kPa to 101.325 kPa, each at a concentration of  $13.93 \pm 0.05 \mu\text{mol/mol C}_2\text{H}_6$ , can be found in Fig. 2. The SNR is the lowest for the 0.666 kPa case, and increases to over 7000 for 101.325 kPa. The effect of pressure broadening is obvious by inspecting the evolution of the spectra as one proceeds from top (Fig. 2a) to bottom (Fig. 2e) in the direction of increasing pressure. The splitting of the Q-branch is only partially resolved at 39.997 kPa and is lost entirely by 101.325 kPa. Many weaker features are relatively intense at low pressure and unresolved at higher pressures. The two sharp features at  $5950.62 \text{ cm}^{-1}$  and  $5950.77 \text{ cm}^{-1}$  become a single broad feature at atmospheric pressure. These two features may be useful for high ethane mole fraction samples at low pressure because of their relative isolation in this dense spectrum. We did not attempt to determine pressure broadening coefficients due to difficulty in fitting such complicated spectra.

The uncertainty components of the determined cross sections are reported in Table 2. We also report the combined uncertainty based on the quadrature sum of all component uncertainties. In the case of low pressures of pure ethane, the relative uncertainty in the measured absorption coefficient (which we refer to as the spectroscopic uncertainty) and the relative systematic (Type B) uncertainty in the pressure measurement are nearly equal. However, the measured pressure increased linearly by nearly 1% with time (a magnitude of 20 mPa) over the course of the pressure determination, significantly increasing the combined uncertainty of the measurement. We observed that the ring-down decay times at a given wavelength did not change systematically, indicating that the increase in pressure was likely due a small leak or to

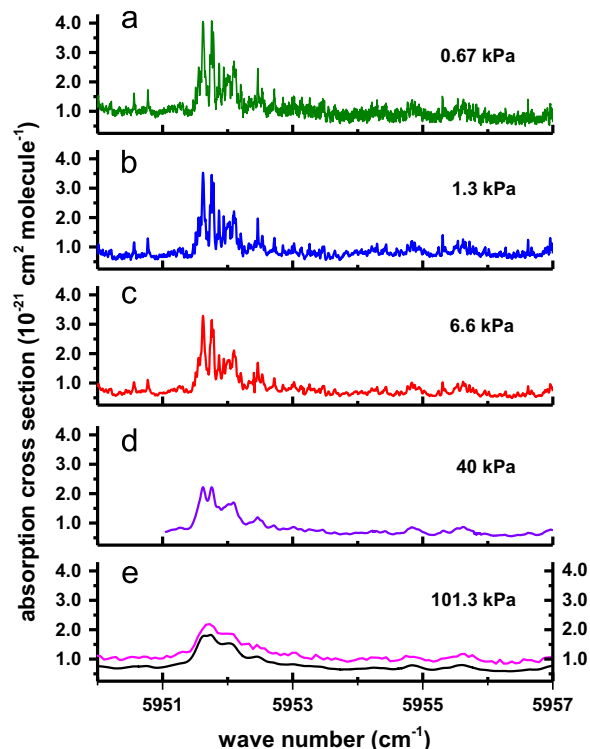


**Fig. 2.** FS-CRDS measurements of ethane-in-air absorption spectra at the indicated pressures. Each of these spectra was acquired with a continuous cavity lock, yielding an uncertainty of nominally 200 kHz in the frequency axis. Spectrum (e) includes a comparison to previously measured FTS spectra of ethane in nitrogen (top trace) at the same pressure [22], offset by  $0.2 \times 10^{-21} \text{ cm}^2 \text{ molecule}^{-1}$  for clarity.

desorption of a non-absorbing species from the spectrometer walls. We have previously observed desorption of  $\text{CO}_2$  and  $\text{H}_2\text{O}$  from the cell walls and consider this a likely source of the observed pressure increase. For the ethane-in-air samples, the uncertainty in molar fraction ( $\sim 0.35\%$ ) limits the accuracy of the measured absorption coefficients. We note that the combined uncertainty could be reduced substantially if one were to employ a mixture with a more accurately known composition. The uncertainty due to etalon effects is included for the peaks of the lines only. The uncertainty increases significantly away from the peaks due to the relative magnitude of the absorption against the relatively constant magnitude of the etalons. The uncertainty at each frequency may be found in the [Supplementary information](#).

The measured absorption cross section of ethane in air ( $13.93 \pm 0.05 \mu\text{mol/mol C}_2\text{H}_6$ ) at 101.3 kPa can be found in

**Table 2**

1 sigma component uncertainties for absorption cross sections measured by FS-CRDS.

	FS-CRDS (%)	Pressure (%)	Temperature (%)	Molar fraction (%)	Etalons at absorption peaks (%)	Combined (%)
<b>Ethane in air (kPa)</b>						
0.6666	0.05	0.01	0.01	0.36	0.86	0.93
1.333	0.05	0.38	0.01	0.36	0.50	0.76
6.666	0.05	0.095	0.02	0.36	0.10	0.39
39.996	0.05	0.022	0.02	0.36	0.02	0.41
101.325	0.05	0.015	0.02	0.36	0.01	0.43
<b>Pure ethane (Pa)</b>						
2.86	0.05	0.045	0.01	< 0.001	< 0.01	0.96*

\* The combined uncertainty for the pure ethane is dominated by the 0.96% relative standard uncertainty assigned to wall desorption effects.

Fig. 2e, along with a comparison to existing FTS spectra of ethane in nitrogen [22]. The CRDS data was recorded at 296.1 K, and the FTS data was recorded at 101.3 kPa and a nearly identical 296 K. The FT resolution was  $0.1125 \text{ cm}^{-1}$ . The FTS spectrum was offset by  $0.2 \times 10^{-21} \text{ cm}^2 \text{ molecule}^{-1}$  for clarity. Most features are clearly similar, with some offset in the baseline (likely due to baseline correction in the FT spectrum). The splitting of the Q-branch is still slightly evident in the FS-CRDS spectrum, but is not resolved in the FT. The smaller features are mostly lost in the noise in the FT, but clearly resolved in the CRDS.

For atmospheric sensing, the  ${}^1\text{Q}_0$ -branch at  $5951.74 \text{ cm}^{-1}$  presents an attractive option for laser-based sensors, with a peak absorption cross section of  $1.82 \times 10^{-21} \text{ cm}^2 \text{ molecule}^{-1}$  at atmospheric pressure. For a 1 s averaging time we estimate a detection limit of 220 pmol/mol, corresponding to a SNR of  $\sim 5$  for the average atmospheric molar fraction of about  $1 \text{ nmol mol}^{-1}$ . Ethane concentrations in plumes from seeps or pipeline leaks would be significantly higher thus leading to commensurately higher SNRs. For example, ethane molar fractions as high as 0.1% were detected in a recent study of pipeline leaks near Washington DC [13].

Ethane is often accompanied by methane in real gas samples [12,13], and the ethane-to-methane ratio provides valuable information about the source of these hydrocarbons. To spectroscopically measure these mixtures, the relevant lines must be spectrally isolated and have absorption coefficients (at the relevant molar-fraction ratios) that are within the dynamic range of the spectrometer. Fig. 3 is a simulated spectrum showing the absorption coefficient of 70.8 nmol/mol of ethane and  $1.8 \mu\text{mol/mol}$  of methane at a pressure of 101.3 kPa. This 3.9% ethane-to-methane ratio for this gas mixture is representative of pipeline-quality dry natural gas in the Washington DC area. Measuring this ethane-to-methane ratio presents a useful test of the ability of a spectrometer to distinguish pipeline leaks above ambient methane levels. This ratio may be employed for source apportionment, which cannot be accomplished solely by measuring the  ${}^{12}\text{CH}_4$  concentration. The methane spectrum is simulated using HITRAN 2012 parameters [34] and the ethane spectrum is based on the present measurements. The most intense nearby methane transition is located at  $\nu_1 = 5949.567 \text{ cm}^{-1}$  (Fig. 3a) and has an absorption coefficient approximately three orders of magnitude larger than the most intense ethane transition,

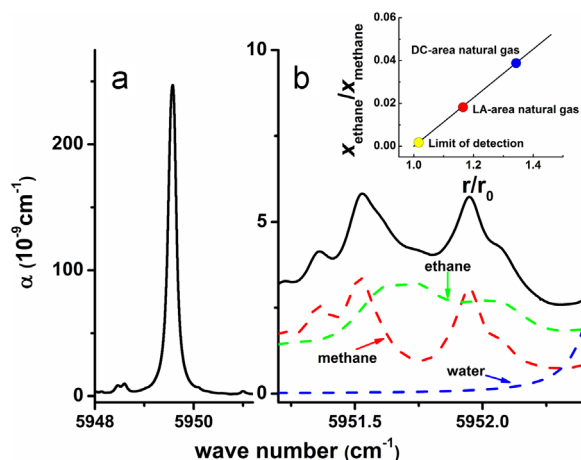


**Fig. 3.** Simulated absorption spectra for mixtures of ethane, methane and water vapor in air. Methane and water vapor spectra are based on HITRAN 2012 [33] line parameters and ethane cross sections are based on the present work. Calculations assume  $p = 101 \text{ kPa}$ ,  $T = 296 \text{ K}$ , and molar fractions of ethane, methane and water of  $32 \text{ nmol mol}^{-1}$ ,  $1.8 \mu\text{mol mol}^{-1}$  and  $20 \mu\text{mol mol}^{-1}$ , respectively. (a) Methane line at  $\nu_1 = 5949.567 \text{ cm}^{-1}$ ; (b) total absorption coefficient (solid black line) corresponding to the sum of ethane, methane and water contributions (each indicated by the labeled dashed lines). Inset: ethane/methane molar fraction ratio plotted as function of  $r/r_0$  (line) in which  $r$  is the measured ratio of absorption coefficients given by Eq. (3) and  $r_0$  is the ratio of methane absorption cross sections  $\sigma_m(\nu_2)/\sigma_m(\nu_1)$  where  $\nu_1 = 5949.567 \text{ cm}^{-1}$  and  $\nu_2 = 5951.72 \text{ cm}^{-1}$ . Here,  $\sigma_e(\nu_2) = 1.81 \times 10^{-21} \text{ cm}^2$ ,  $\sigma_m(\nu_1) = 5.12 \times 10^{-20} \text{ cm}^2$  and  $\sigma_m(\nu_2) = 2.05 \times 10^{-22} \text{ cm}^2$ . The labeled symbols indicate pipeline-quality natural gas ethane-to-methane ratios in Washington DC and the Los Angeles region as well as the minimum detectable ethane-to-methane ratio of the FS-CRDS spectrometer used in this study.

concentration of methane. The ethane  ${}^1\text{Q}_0$  branch itself is partially blended with the wings of the primary transition along with weaker methane transitions. However, the absorption coefficient at the peak of the methane transition at  $\nu_1$  could be measured on the present FS-CRDS spectrometer with a  $\text{SNR} > 20,000$  and used to tightly constrain the overlapping ethane and methane absorption features at  $\nu_2 = 5951.74 \text{ cm}^{-1}$ . This approach would allow accurate measurement of ethane molar fractions and ethane-to-methane ratios in real air mixtures. The ethane-to-methane molar fraction ratio  $x_e/x_m$  can be determined by

$$\frac{x_e}{x_m} = \frac{r\sigma_m(\nu_1) - \sigma_m(\nu_2)}{\sigma_e(\nu_2)}, \quad (3)$$

where  $r = (\alpha(\nu_2)/\alpha(\nu_1))$  is a measured ratio of absorption coefficients, and where  $\sigma_m$  and  $\sigma_e$  represent the absorption cross sections of air-broadened methane and ethane, respectively, at the indicated wave numbers. We note that  $r$  is independent of the absolute concentration of methane or ethane, because it is proportional to the ratio of their abundances.

The spectroscopic contribution of atmospheric water vapor at  $\nu_2$  (wave number used to probe ethane) is an additional consideration. Moist atmospheric air, with a water molar fraction of 1% would have an absorption coefficient of  $5.6 \times 10^{-9} \text{ cm}^{-1}$  at this wave number, which is not negligible compared to absorption by the ethane and methane. Because the molar fraction of water vapor cannot be easily constrained in such a gas mixture, drying the air sample would significantly increase measurement sensitivity and accuracy. Commercially available membrane driers can reliably dry air to a dew point temperature below  $-50^\circ \text{C}$  (corresponding to  $20 \mu\text{mol/mol}$  of  $\text{H}_2\text{O}$ ), while quantitatively retaining methane and ethane. At this concentration, the absorption coefficient of water vapor would be significantly lower than that of ethane. The absorption coefficient for  $20 \mu\text{mol/mol}$  of water vapor is shown in Fig. 3b, along with the summation of all absorbers. The combined spectrum demonstrates that a spectrometer of reasonable sensitivity could resolve ethane in realistic samples of pipeline-natural-gas in air at this wavelength. Real samples would also contain other hydrocarbons, such as propane. The propane/ethane ratio of pipeline quality natural gas is roughly 0.1 mol propane/mol ethane [12], and the absorption spectrum of propane is broad and fairly weak ( $\sim 5 \times 10^{-22} \text{ cm}^2 \text{ molecule}^{-1}$ ) in this spectral region [22]. The effect on the sensor's ability to measure the methane to ethane ratio should be minimal.

The inset of Fig. 3b illustrates the ability of this spectrometer to detect and differentiate sources of pipeline-quality natural gas leaks. Assuming a constant methane background of  $1.8 \mu\text{mol mol}^{-1}$ , the lowest detectable ethane-to-methane ratio is 0.15%. This corresponds to an ethane molar fraction of  $2.9 \text{ nmol mol}^{-1}$ , which is only three times greater than the natural abundance value. While not able to measure ethane at atmospheric-background concentration levels, this approach would provide a highly sensitive and wide dynamic range measurement for tracking fugitive pipeline emissions containing elevated amounts of ethane.

#### 4. Conclusion

We have measured the cross sections of pure ethane and ethane in air in the wave number region from  $5950 \text{ cm}^{-1}$  to  $5967 \text{ cm}^{-1}$  using frequency-stabilized cavity ring-down spectroscopy. Measurements were performed at a variety of pressures, from the Doppler-broadened region for pure ethane up to 101.3 kPa for ethane in air. The measured line positions are in good agreement with existing FTS spectra, but the higher spectral resolution and greater sensitivity of our spectrometer reveal significant differences in absorption cross sections at low pressure. We have resolved many weak

features, which may prove useful for performing global fits of the complicated ethane spectrum. The complete list of absorption cross sections and uncertainties at a frequency sampling interval of 109 MHz is reported.

The  ${}^1\text{Q}_0$  transition, with a cross section of  $1.81 \times 10^{-21} \text{ cm}^2 \text{ molecule}^{-1}$  at atmospheric pressure, is a viable candidate for detection of ethane in the atmosphere, especially for detection of fugitive natural gas emissions. We have demonstrated that a suitably sensitive spectrometer, such as the one employed in this study, could detect ethane at a level that is relevant to the detection of pipeline-quality natural gas plumes in atmospherically relevant mixtures containing methane, ethane, and water vapor.

#### Acknowledgments

This work was supported by the Greenhouse Gas and Climate Sciences Measurements Program of the National Institute of Standards and Technology.

#### Appendix A. Supporting information

Supplementary data associated with this article can be found in the online version at <http://dx.doi.org/10.1016/j.jqsrt.2015.03.010>.

#### References

- Simpson IJ, Anderson MPS, Meinardi S, Bruhwiler L, Blake NJ, Helming D, et al. Long-term decline of global atmospheric ethane concentrations and implications for methane. *Nature* 2012;448(7412):490.
- Blasing TJ. Recent greenhouse gas concentrations. Carbon Dioxide Information Analysis Center. 10.3334/CDIAC/atg.032; 2014.
- Aikin AC, Herman JR, Majer EJ, Mcquillan CJ. The atmospheric chemistry of ethane and ethylene. *J Geophys Res* 1982;87:3105–18.
- Singh HB, Hanst PL. Peroxyacetyl nitrate (PAN) in the unpolluted atmosphere: an important reservoir for nitrogen oxides. *Geophys. Res. Lett.* 1981;8:941.
- Jacob DJ. Introduction to atmospheric chemistry. Princeton University Press; 1999.
- Boissard C, Bonsang B, Kanakidou M, Lambert G. TROPOZ II: global distributions and budgets of methane and light hydrocarbons. *J. Atmos. Chem* 1996;25:115.
- Xiao Y, Logan JA, Jacob DJ, Hudman RC, Yantosca R, Blake DR. Global budget of ethane and regional constraints on US sources. *J Geophys Res* 2008;113:D21306.
- Xiao Y, Jacob DJ, Wang JS, Logan JA, Pamer PI, Suntharakingam P. Constraints on Asian and European sources of methane from  $\text{CH}_4\text{-C}_2\text{H}_6\text{-CO}$  correlations in Asian outflows. *J Geophys Res* 2004;109:D15S16.
- Stein O, Rudolph J. Modeling and interpretation of stable carbon isotope ratios of ethane in global chemical transport models. *J Geophys Res* 2007;112:D14308.
- Olivier J., Peters J., Granier C., Pétron G., Müller J.F., Wallens, S., Present and future surface emissions of atmospheric compounds. POET Report #2. EU project EVK2-1999-00011; 2003.
- Etioppe G, Ciccioli P. Earth's degassing: a missing ethane and propane source. *Science* 2009;323:478.
- Peischl J, Ryerson TB, Brioude J, Aikin KC, Andrews AE, Atlas E, et al. Quantifying sources of methane using light alkanes in the Los Angeles basin, California. *J Geophys Res Atmos* 2013;118(10):4974–90.
- Jackson RB, Down A, Phillips NG, Ackley RC, Cook CW, Plata DL, et al. Natural gas pipeline leaks across Washington, DC. *Environ Sci Technol* 2014;48(3):2051–8.
- Kim SJ, Geballe TR, Seo HJ, JKima JH. Jupiter's hydrocarbon polar brightening: discovery of 3-micron line emission from solar polar  $\text{CH}_4$ ,  $\text{C}_2\text{H}_2$ , and  $\text{C}_2\text{H}_6$ . *Icarus* 2009;202:354–7.

- 15 Herman BE, Jennings DE, Sada PV, Bjoraker GL, Achterberg RK, Simon-Miller A-A, et al. Saturn's latitudinal C<sub>2</sub>H<sub>2</sub> and C<sub>2</sub>H<sub>6</sub> abundance profiles from Cassini/CIR Sand ground-based observations. *Icarus* 2009;249–59.
- 16 Brown RH, Soderblom LA, Soderblom JM, Clark RN, Jaumann R, Barnes JW. The identification of liquid ethane in Titan's Ontario Lacus. *Nature* 2008;454:607–10.
- 17 Griffith CA, Penteado P, Rannou P, Brown R, Boudon V, Baines KH, et al. Evidence for a polar ethane cloud on Titan. *Science* 2006;313:1620.
- 18 Griffith CA, Penteado P, Baines K, Drossart P, Barnes J, Bellucci G, et al. The evolution of Titan's mid-latitude clouds. *Science* 2005;310(5747):474–7.
- 19 Bohnhardt H, Mumma MJ, Villanueva GL, DiSanti MA, Bonev BP, Lippi M, et al. The unusual volatile composition of the Halley-type comet 8P/Tuttle: addressing the existence of an inner Oort Cloud. *Astrophys J* 2008;683:L71.
- 20 Harrison JJ, Nicholas DCA, Bernath PF. Infrared absorption cross sections for ethane (C<sub>2</sub>H<sub>6</sub>) in the 3 μm region. *J Quant Spectrosc Radiat Transf* 2010;111:357.
- 21 Smith LG. The infra-red spectrum of C<sub>2</sub>H<sub>6</sub>. *J Chem Phys* 1949;17:139.
- 22 Laboratory PNN. (<http://www.pnl.gov>).
- 23 Hepp M, Herman M. Vibration–rotation bands in ethane 2000;98:57–61 *Mol Phys* 2000;98:57–61.
- 24 Hepp M, Herman M. The jet cooled spectrum of ethane between 4000 and 4500 cm<sup>-1</sup>. *Mol Phys* 1998;94:829–38.
- 25 Skeldon KD, McMillan LC, Wyse CA, Monk SD, Gibson G, Patterson C, et al. Application of laser spectroscopy for measurement of exhaled ethane in patients with lung cancer. *Respir Med* 2006;100(2):300–6.
- 26 Skeldon KD, Gibson GM, Wyse CA, McMillan LC, Monk SD, Longbottom C, et al. Development of high-resolution real-time sub-ppb ethane spectroscopy and some pilot studies in life science. *Appl Opt* 2005;44(22):4712–21.
- 27 Ngai AKY, Persijn ST, von Basum G, Harren FJM. Automatically tunable continuous-wave optical parametric oscillator for high-resolution spectroscopy and sensitive trace-gas detection. *Appl Phys B* 2006;85(2–3):173–80.
- 28 Oh M-K, Lee Y-H, Choi S-C, Ko D-K, Lee J-M. Detection of methane and ethane by continuous-wave cavity ring-down spectroscopy near 1.67 μm. *J Opt Soc Korea* 2008;12(1):1–6.
- 29 von Basum G, Halmer D, Hering P, Mürtz M, Schiller S, Müller F, et al. Parts per trillion sensitivity for ethane in air with an optical parametric oscillator cavity leak-out spectrometer. *Opt Lett* 2004;29(8):797–9.
- 30 Arslanov DD, Swinkels K, Cristescu SM, Harren FJM. Real-time, subsecond, multicomponent breath analysis by Optical Parametric Oscillator based Off-Axis Integrated Cavity Output Spectroscopy. *Opt Express* 2011;19(24):24078–89.
- 31 Hodges JT, Ciurylo R. Automated high-resolution frequency-stabilized cavity ring-down absorption spectrometer. *Rev Sci Instrum* 2005;76:023112.
- 32 Hodges JT, Layer HP, Miller WW, Scace GE. Frequency stabilized single mode cavity ringdown apparatus for high resolution absorption spectroscopy. *Rev Sci Instrum* 2004;75(4):849–63.
- 33 Long DA, Cygan A, van Zee RD, Okumura M, Miller CE, Lisak D, et al. Frequency-stabilized cavity ring-down spectroscopy. *Chem Phys Lett* 2012;536(0):1–8.
- 34 Rothman LS, Gordon IE, Babikov Y, Barbe A, Benner DC, Bernath PF, et al. The HITRAN2012 molecular spectroscopic database. *J Quant Spectrosc Radiat Transf* 2013;130:4–50.
- 35 Brown LR, Farmer CB, Rinsland CP, et al. Molecular line parameters for the atmospheric trace molecule spectroscopy experiment. *Appl Opt* 1987;26(23):5154.
- 36 Brown LR, Farmer CB, Rinsland CP, Toth RA. Molecular line parameters for the atmospheric trace molecule spectroscopy experiment. *Appl Opt* 1987;26(23):5154.